



Third-order symplectic integration method with inverse time dispersion transform for long-term simulation



Yingjie Gao ^{a,b}, Jinhai Zhang ^{a,*}, Zhenxing Yao ^a

^a Key Laboratory of Earth and Planetary Physics, Institute of Geology and Geophysics, Chinese Academy of Sciences, Beijing, China

^b University of Chinese Academy of Sciences, Beijing, China

ARTICLE INFO

Article history:

Received 29 November 2015

Received in revised form 11 March 2016

Accepted 12 March 2016

Available online 17 March 2016

Keywords:

Inverse time dispersion transform

Time-dispersion error

Pseudospectral method

Symplectic integration method

Long-term simulation

ABSTRACT

The symplectic integration method is popular in high-accuracy numerical simulations when discretizing temporal derivatives; however, it still suffers from time-dispersion error when the temporal interval is coarse, especially for long-term simulations and large-scale models. We employ the inverse time dispersion transform (ITDT) to the third-order symplectic integration method to reduce the time-dispersion error. First, we adopt the pseudospectral algorithm for the spatial discretization and the third-order symplectic integration method for the temporal discretization. Then, we apply the ITDT to eliminate time-dispersion error from the synthetic data. As a post-processing method, the ITDT can be easily cascaded in traditional numerical simulations. We implement the ITDT in one typical exiting third-order symplectic scheme and compare its performances with the performances of the conventional second-order scheme and the rapid expansion method. Theoretical analyses and numerical experiments show that the ITDT can significantly reduce the time-dispersion error, especially for long travel times. The implementation of the ITDT requires some additional computations on correcting the time-dispersion error, but it allows us to use the maximum temporal interval under stability conditions; thus, its final computational efficiency would be higher than that of the traditional symplectic integration method for long-term simulations. With the aid of the ITDT, we can obtain much more accurate simulation results but with a lower computational cost.

© 2016 The Authors. Published by Elsevier Inc. This is an open access article under the CC BY-NC-ND license (<http://creativecommons.org/licenses/by-nc-nd/4.0/>).

1. Introduction

Seismic modeling is an important foundation for exploration seismology, and synthetic seismograms are helpful for understanding wave phenomena in complex media. High-accuracy seismic modeling schemes are essential for high-resolution seismic interpretations. Seismic modeling methods can be classified into three main categories: direct methods, integral-equation methods, and ray-tracing methods [1]. The direct methods are the most popular since they can handle complicated wave phenomena associated with various structures well. The direct methods include three main kinds: finite-difference (FD) methods [2–4], pseudospectral methods [5–8], and finite-element methods [9]. Some hybrid methods, such as spectral-element methods [10] and finite-volume methods [11] have also been developed to achieve a much higher accuracy in numerical simulations.

* Corresponding author. Tel.: +86 10 82998440.
E-mail address: zjh@mail.iggcas.ac.cn (J. Zhang).

For direct seismic modeling methods, both space and time variables need to be discretized. A large sampling interval of discretization would bring severe numerical dispersion error; in contrast, a small sampling interval could reduce the numerical dispersion error but would greatly increase the computational cost. Therefore, it is necessary to develop high accuracy methods that can employ coarse grids in both temporal and spatial discretizations. Conventional FD schemes for spatial discretization lead to space dispersion error when computing the space derivatives of the wave equations. A typical exhibition of the space dispersion error is that the high frequency components of the wavefields do not propagate exactly with the expected velocity [12]. Numerous methods have been developed to eliminate space dispersion: the high-order FD schemes [12–16], optimized FD operators [17–26], the flux-corrected transport technique [27–29], the nearly analytical discrete methods [30,31], the stereo-modeling methods [32], and the pseudospectral methods [5–8].

Numerical discretization of temporal derivatives also introduces numerical artifacts, which are called time-dispersion error. The time-dispersion error is not as serious as the space dispersion error since it can be greatly reduced using a fairly small temporal interval. However, in the presence of long-term problems and large-scale models, a small temporal interval would tremendously increase the computational cost; for such cases, we have to use a large temporal interval to avoid overburdened computational cost. Unfortunately, a large temporal interval would introduce strong time-dispersion error as expected. For example, the second-order FD discretization have been widely used [33] due to its simplicity, but an extremely fine temporal interval is needed to minimize the time-dispersion error since its time-dispersion error is the most serious among all known methods.

To cope with the time-dispersion error, various methods have been developed, such as high-order time FD schemes [12, 34–37], the rapid expansion method [38–41], low rank methods [42,43], Fourier finite-difference methods [44–46], correction methods based on filter and interpolation [47–50], and time dispersion transforms [51,52] as reviewed below.

Chen [34] presented three modeling schemes using high-order temporal discretization: the Lax–Wendroff method [1,12, 53], the Nyström method [54–56], and the splitting method [57–59]. The splitting method is the same as the third-order symplectic integration method developed by Ruth [57]. Zhang et al. [35] and Zhang and Zhang [37] proposed a one-step extrapolation algorithm. This algorithm formulates the two-way wave equation as a first-order partial differential equation in time without suffering from numerical instability or time dispersion problems, which allows for a large temporal interval. However, their decomposition algorithm, optimized separable approximation [60], is expensive due to too many Fourier transforms [61].

Fomel et al. [42] approximated the wave extrapolation operators using the low rank approximation of a matrix operator in the mixed space-wavenumber domain. This method reduces computational cost by optimally selecting reference velocities and weights [61]. Song and Fomel [44] developed a related method, the Fourier finite-difference method, by cascading a Fourier transform operator and an FD operator to form a chain operator. The Fourier finite-difference method may have an advantage in efficiency because it uses only one pair of multidimensional forward and inverse fast Fourier transforms per temporal interval. However, it does not offer flexible controls on the approximation accuracy [43].

The rapid expansion method [39–41] incorporates Chebyshev polynomials during the approximation. This method employs many high orders for the temporal discretization (e.g., 8-order [40]) thus is suitable for large temporal intervals using concepts similar to the work presented by Tal-Ezer et al. [38]. Instead of using more terms in the expansion, Etgen and Brandsberg-Dahl [62] generalize the pseudospectral method to obtain pseudo-analytical solutions. They modify the Fourier transform of the Laplacian operator for the constant velocity model in an arbitrary number of space dimensions.

The time dispersion has proven to be independent of both the velocity model and the space dispersion model; furthermore, it is predictable since it only depends on the frequency, temporal interval, and propagation time [50]. Therefore, the time dispersion could be handled separately from space dispersion, without considering velocity variations. Liu et al. [49] formulated an explicit time evolution scheme in the time–space domain by introducing a cosine function approximation, in which optimum stencils and least-squares coefficients are introduced. Stork [48] proposed that the time-dispersion error is fully predictable and can be removed with careful filtering after FD modeling. Time dispersion is fixed by applying a time variable filter and interpolation. Dai et al. [50] showed more details and extended the mathematical analyses on Stork's work. Li et al. [47] showed two post-propagation filtering schemes based on the method proposed by Stork [48], and this type of correction method does not affect the computational efficiency much.

Wang and Xu [51,52] studied the time dispersion of pseudospectral methods and predicted it in theory. To remove the time-dispersion error, they proposed a time dispersion prediction algorithm (i.e. forward time dispersion transform) and correction algorithm (i.e. inverse time dispersion transform), which works for any order conventional time FD scheme. A relatively large temporal interval is allowed for wave propagation, which can greatly retain the computational efficiency while improving the accuracy [51].

For long-term simulations in large-scale seismic exploration and seismology [34,63–65], the conventional FD schemes on discretizing the temporal derivatives are not structure-preserving thus are extremely difficult to avoid error accumulations caused by the time dispersion. We can solve wave equations using symplectic integration methods (or the Hamiltonian dynamical systems) to reduce error accumulations [57,66,67]. On the other hand, a large temporal interval that is approaching the stability upper limit would greatly improve the computational efficiency. However, symplectic integration methods still suffer from error accumulations at fairly long travel times when using large temporal interval.

In this paper, we incorporate the inverse time dispersion transform (ITDT) [51,52] into the third-order symplectic integration method to reduce error accumulations when using a large temporal interval. We verify the superiority of our scheme by comparing it with the conventional second-order scheme and the rapid expansion method (8-order [40]). The

Table 1
Coefficients of the third-order symplectic integration methods.

	p_1	p_2	p_3	q_1	q_2	q_3
Ruth	$\frac{7}{24}$	$\frac{3}{4}$	$-\frac{1}{24}$	$\frac{2}{3}$	$-\frac{2}{3}$	1
Iwatsu-A	$\frac{-7+\sqrt{209/2}}{12}$	$\frac{11}{12}$	$\frac{8-\sqrt{209/2}}{12}$	$\frac{2}{9}(1+\sqrt{\frac{38}{11}})$	$\frac{2}{9}(1-\sqrt{\frac{38}{11}})$	$\frac{5}{9}$
Iwatsu-B	$\frac{-7-\sqrt{209/2}}{12}$	$\frac{11}{12}$	$\frac{8+\sqrt{209/2}}{12}$	$\frac{2}{9}(1-\sqrt{\frac{38}{11}})$	$\frac{2}{9}(1+\sqrt{\frac{38}{11}})$	$\frac{5}{9}$
MLA	q_3	q_2	q_1	0.919661523017399857	$\frac{1}{4q_1} - \frac{q_1}{2}$	$1 - q_1 - q_2$

computational efficiency is greatly improved since the ITDT allows a large temporal interval that is approaching the stability upper limit without suffering from error accumulations.

2. Pseudospectral method for spatial discretization

The pseudospectral method is used since its error mainly arises from the temporal discretization [6], which is helpful for verifying the performance of different schemes on reducing the time dispersion. For simplicity we consider the 2D acoustic wave equation

$$\frac{\partial^2 u}{\partial t^2} = c^2 \left(\frac{\partial^2 u}{\partial x^2} + \frac{\partial^2 u}{\partial z^2} \right), \tag{1}$$

where $u(x, z, t)$ is the wavefield, and $c(x, z)$ is the velocity. The pseudospectral method for equation (1) reads [6]

$$\frac{\partial^2 u}{\partial t^2} = c^2 \{ F_x^- [-k_x^2 F_x^+(u)] + F_z^- [-k_z^2 F_z^+(u)] \}, \tag{2}$$

where F_x^+ and F_z^+ are 1D forward Fourier transforms along the x - and z -directions, respectively; F_x^- and F_z^- are 1D inverse Fourier transforms along the x - and z -directions, respectively; k_x and k_z are wavenumbers along the x - and z -directions, respectively.

3. Symplectic integration method for temporal discretization

The symplectic properties guarantee that the numerical solution evolves in the same system as the solution of the original continuous differential equation; thus, the symplectic integration methods have a remarkable capability for long-term simulation [56]. The symplectic integration method consists of several substeps for one-step computation [57–59]. A typical symplectic integration method for equation (2) reads [34]

$$\begin{aligned} v^{s(i)} &= v^{s(i-1)} + p_i \Delta t c^2 \{ F_x^- [-k_x^2 F_x^+(u^{s(i-1)})] + F_z^- [-k_z^2 F_z^+(u^{s(i-1)})] \}, \\ u^{s(i)} &= u^{s(i-1)} + q_i \Delta t v^{s(i)}, \quad i = 1, 2, \dots, I, \end{aligned} \tag{3}$$

where the superscripts $s(i)$ denote that the intermediate result, $v^{s(i)}$ is the intermediate variable, and $u^{s(0)} = u^n \approx u(n\Delta t)$, $v^{s(0)} = v^n \approx v(n\Delta t)$, $u^{s(l)} = u^{n+l} \approx u[(n+1)\Delta t]$, and $v^{s(l)} = v^{n+l} \approx v[(n+1)\Delta t]$. There are I substeps needed to obtain the results from time level n to time level $n+1$. The intermediate variables p_i and q_i are the coefficients of the symplectic integration method in the i -th substep.

We concentrate on the third-order symplectic integration method (i.e. $I = 3$), since it is better in accuracy than the second-order one for long-term problems [34]. The complete expression of equation (3) reads [34]

$$\begin{aligned} v^{s(1)} &= v^{s(0)} + p_1 \Delta t c^2 \{ F_x^- [-k_x^2 F_x^+(u^{s(0)})] + F_z^- [-k_z^2 F_z^+(u^{s(0)})] \}, \\ u^{s(1)} &= u^{s(0)} + q_1 \Delta t v^{s(1)}, \\ v^{s(2)} &= v^{s(1)} + p_2 \Delta t c^2 \{ F_x^- [-k_x^2 F_x^+(u^{s(1)})] + F_z^- [-k_z^2 F_z^+(u^{s(1)})] \}, \\ u^{s(2)} &= u^{s(1)} + q_2 \Delta t v^{s(2)}, \\ v^{s(3)} &= v^{s(2)} + p_3 \Delta t c^2 \{ F_x^- [-k_x^2 F_x^+(u^{s(2)})] + F_z^- [-k_z^2 F_z^+(u^{s(2)})] \}, \\ u^{s(3)} &= u^{s(2)} + q_3 \Delta t v^{s(3)}, \end{aligned} \tag{4}$$

where $p_1, p_2, p_3, q_1, q_2,$ and q_3 are the coefficients for the third-order symplectic integration method. The values of the coefficients p_i and q_i were first given by Ruth [57]. McLachlan and Atela [68] derived a new set of optimized coefficients based on the minimum truncation error method [69]. Iwatsu [70] gave two new solutions by modifying the solving algorithm that given by Ruth [57]. We call the coefficients given by Ruth [57], McLachlan and Atela [68], and Iwatsu [70] the following names: Ruth, MLA, Iwatsu-A, Iwatsu-B, respectively. These four sets of coefficients are shown in Table 1.

Table 2
Stability upper limits ν_0 and time dispersion upper limits when $|\theta(\omega, \Delta t) - \omega\Delta t| < 5 \times 10^{-4}$ for different schemes. Number in the parentheses represents the points per period $T = 2\pi/\nu$.

	ν_0	$\nu(\theta(\omega, \Delta t) - \omega\Delta t < 5 \times 10^{-4})$
2-order	2 (3.14159)	0.2285 (27.4975)
Ruth	2.50748 (2.50748)	0.9197 (6.8318)
Iwatsu-A	2.66590 (2.35687)	1.1699 (5.3707)
Iwatsu-B	1.57278 (3.99495)	0.3751 (16.7507)
MLA	4.52009 (1.39006)	1.0753 (5.8432)

4. Stability condition

We first make a simple variable transform $\bar{v}^{s(i)} = \Delta t v^{s(i)}$ in order to obtain polynomials in terms of $ck\Delta t$. Equation (3) can be expressed as

$$\begin{aligned} \bar{V}^{s(i)} &= \bar{V}^{s(i-1)} - p_i \Delta t^2 c^2 k^2 U^{s(i-1)}, \\ U^{s(i)} &= U^{s(i-1)} + q_i \bar{V}^{s(i)}, \quad i = 1, 2, \dots, I, \end{aligned} \tag{5}$$

where \bar{V} and U are the Fourier transformation of \bar{v} and u , respectively. Equation (5) is equivalent to

$$\begin{bmatrix} \bar{V}^{s(i)} \\ U^{s(i)} \end{bmatrix} = \overbrace{\begin{bmatrix} 1 & -p_i \Delta t^2 c^2 k^2 \\ q_i & 1 - p_i q_i \Delta t^2 k^2 \end{bmatrix}}^{M_i} \begin{bmatrix} \bar{V}^{s(i-1)} \\ U^{s(i-1)} \end{bmatrix}, \quad i = 1, 2, \dots, I, \tag{6}$$

where the transformation matrix M is expressed as [70]

$$M = M_3 M_2 M_1 = \begin{bmatrix} 1 + a_{11} \nu^2 + b_{11} \nu^4 & a_{12} \nu^2 + b_{12} \nu^4 + c_{12} \nu^6 \\ a_{21} + b_{21} \nu^2 + c_{21} \nu^4 & 1 + a_{22} \nu^2 + b_{22} \nu^4 + c_{22} \nu^6 \end{bmatrix},$$

with

$$\begin{aligned} a_{11} &= -(p_2 q_1 + p_3 q_2 + p_3 q_1), & b_{11} &= p_2 p_3 q_1 q_2, \\ a_{12} &= -(p_1 + p_2 + p_3), & b_{12} &= p_1 p_2 q_1 + p_1 p_3 q_2 + p_1 p_3 q_1 + p_2 p_3 q_2, \\ c_{12} &= -p_1 p_2 p_3 q_1 q_2, \\ a_{21} &= q_1 + q_2 + q_3, & b_{21} &= -(p_2 q_1 q_3 + p_2 q_1 q_2 + p_3 q_2 q_3 + p_3 q_1 q_3), \\ c_{21} &= p_2 p_3 q_1 q_2 q_3, \\ a_{22} &= -(p_1 q_3 + p_2 q_3 + p_1 q_2 + p_1 q_1 + p_2 q_2 + p_3 q_3), \\ b_{22} &= p_1 p_2 q_1 q_3 + p_1 p_2 q_1 q_2 + p_1 p_3 q_1 q_3 + p_2 p_3 q_2 q_3, \\ c_{22} &= -p_1 p_2 p_3 q_1 q_2 q_3, \end{aligned}$$

$\nu = ck\Delta t = \omega\Delta t$, and $\omega = 2\pi f$ (f is the frequency). To obtain the eigenvalue λ of M , we can solve

$$\lambda^2 - \text{tr}(M)\lambda + \det(M) = 0, \tag{7}$$

where $\text{tr}(M)$ is the trace of matrix M , and $\det(M)$ is the determinant of matrix M . The solution of equation (7) is

$$\lambda = \frac{\text{tr}(M)}{2} \pm \sqrt{\left[\frac{\text{tr}(M)}{2}\right]^2 - \det(M)}, \tag{8}$$

where

$$\begin{aligned} \text{tr}(M) &= 2 - (p_1 q_1 + p_2 q_1 + p_3 q_1 + p_1 q_2 + p_2 q_2 + p_3 q_2 + p_1 q_3 + p_2 q_3 + p_3 q_3) \nu^2 \\ &\quad + (p_1 p_2 q_1 q_2 + p_2 p_3 q_1 q_2 + p_1 p_2 q_1 q_3 + p_1 p_3 q_1 q_3 + p_1 p_3 q_2 q_3 + p_2 p_3 q_2 q_3) \nu^4 - p_1 p_2 p_3 q_1 q_2 q_3 \nu^6, \end{aligned}$$

and $\det(M) = 1$.

The stability limit for equation (4) is obtained by requiring $|\lambda| \leq 1$. Table 2 shows the stability upper limits ν_0 of ν for five schemes: (a) the traditional pseudospectral method with the second-order time FD discretization [6], which is abbreviated as '2-order'; (b) Ruth; (c) Iwatsu-A; (d) Iwatsu-B; and (e) MLA. Obviously, the stability upper limit of Iwatsu-B is the smallest (even smaller than that of 2-order); and the stability upper limit of MLA is the largest among all of the five schemes.

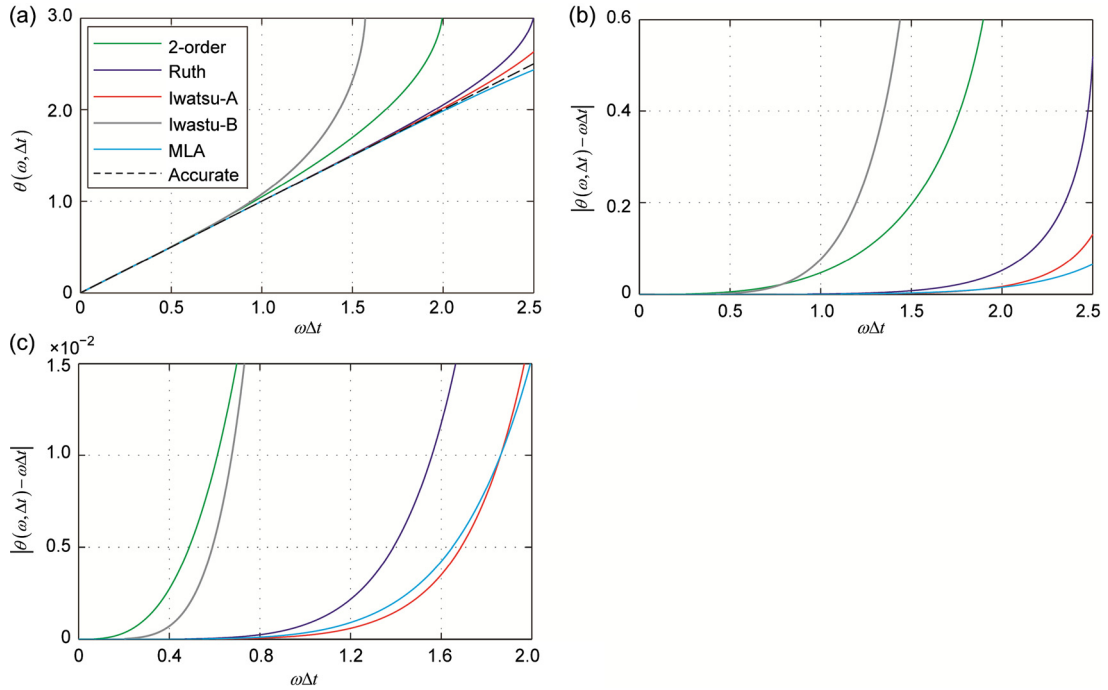


Fig. 1. Comparison between the phase shift $\theta(\omega, \Delta t)$ and the theoretical phase shift $\omega\Delta t$ for the second-order time FD scheme as well as several third-order symplectic integration schemes. (a) is the phase shift $\theta(\omega, \Delta t)$ for different schemes; (b) is the dispersion error $|\theta(\omega, \Delta t) - \omega\Delta t|$ for different schemes; (c) is an enlarged portion of (b).

5. Inverse time dispersion transform

Denoting the amplitude of the wave propagation by a constant vector $[A_1, A_2]^T$, the expression $[\bar{V}^n, U^n]^T$ in equation (6) can be decomposed into

$$\begin{bmatrix} \bar{V}^n \\ U^n \end{bmatrix} = \begin{bmatrix} A_1 \\ A_2 \end{bmatrix} \exp[i(\omega t - k_x x - k_z z)].$$

Similarly, $[\bar{V}^{n+1}, U^{n+1}]^T$ can be decomposed into

$$\begin{bmatrix} \bar{V}^{n+1} \\ U^{n+1} \end{bmatrix} = \begin{bmatrix} A_1 \\ A_2 \end{bmatrix} \exp[i(\omega(t + \Delta t) - k_x x - k_z z)] = \begin{bmatrix} \bar{V}^n \\ U^n \end{bmatrix} \exp(i\omega\Delta t).$$

Equation (6) can be rewritten as

$$\begin{bmatrix} \bar{V}^{n+1} \\ U^{n+1} \end{bmatrix} = M \begin{bmatrix} \bar{V}^n \\ U^n \end{bmatrix} = \lambda \begin{bmatrix} \bar{V}^n \\ U^n \end{bmatrix},$$

thus, we have $\lambda = \exp(i\omega\Delta t)$. According to

$$\exp(i\omega\Delta t) = \cos(\omega\Delta t) + i \sin(\omega\Delta t) = \cos(\omega\Delta t) + \sqrt{\cos^2(\omega\Delta t) - 1},$$

which has the same form as equation (8); thus, we can obtain the time dispersion of equation (4) as

$$\cos(\omega\Delta t) = \frac{\text{tr}(M)}{2}. \tag{9}$$

If we consider $\omega\Delta t$ on the left side of equation (9) as a function of $\theta(\omega, \Delta t)$, it should be expressed as [51]

$$\theta(\omega, \Delta t) = \arccos\left(\frac{\text{tr}(M)}{2}\right). \tag{10}$$

Fig. 1(a) shows the comparison between the phase shift $\theta(\omega, \Delta t)$ of different schemes and the theoretical phase shift $\omega\Delta t$ according to equation (10). When the circular frequency ω is low and the temporal interval Δt is small enough, $\theta(\omega, \Delta t)$ is close to $\omega\Delta t$. **Fig. 1(b)** shows the absolute time-dispersion error $|\theta(\omega, \Delta t) - \omega\Delta t|$, which would grow up with an increasing temporal interval and circular frequency.

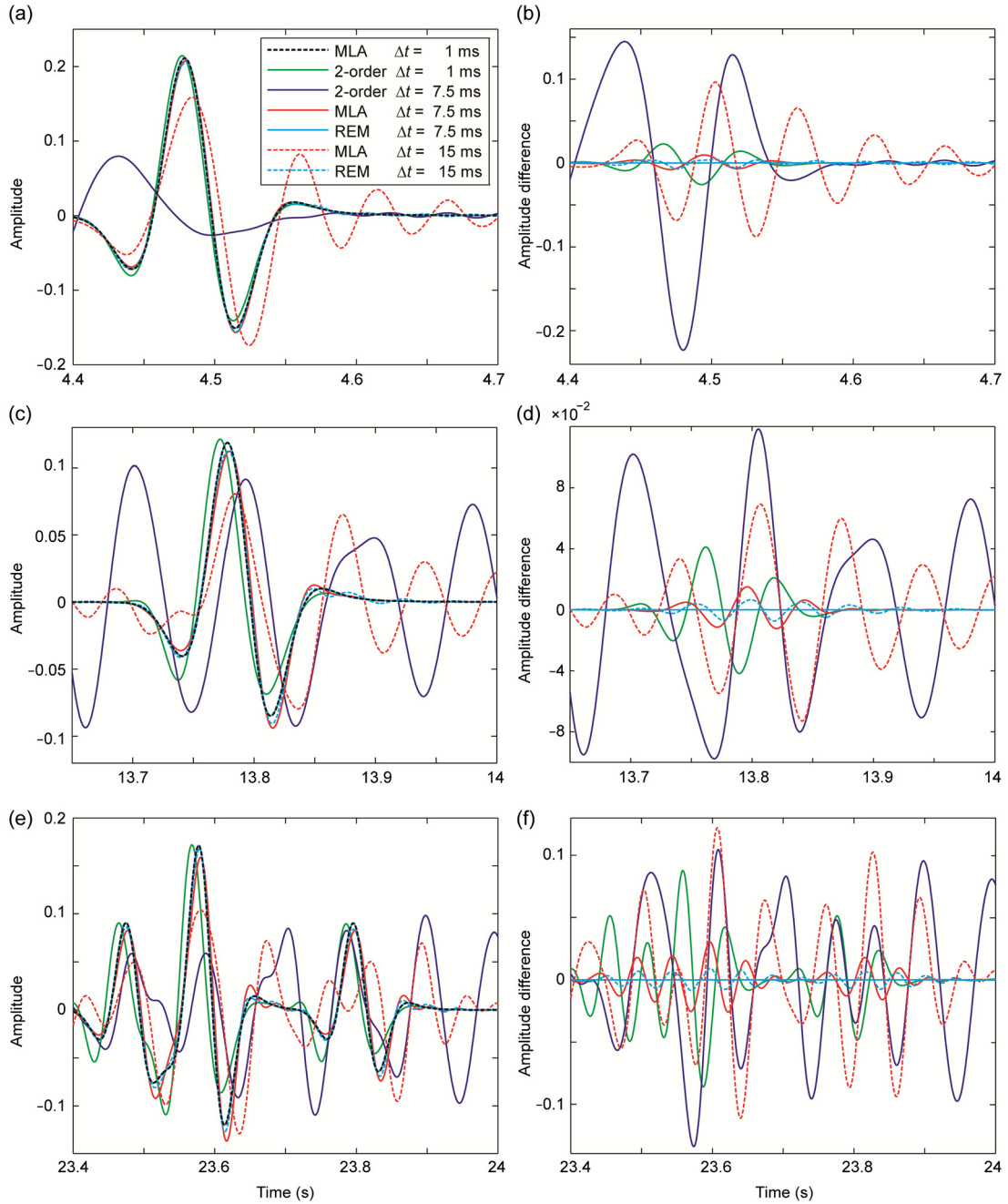


Fig. 2. Waveforms and the amplitude errors. The traces are recorded at a fixed point ($x = -3000$ m, $z = 3000$ m). (a), (c), and (e) are waveforms around 4.5, 13.8, and 23.7 s, respectively; (b), (d), and (f) are amplitude differences between different schemes and MLA with $\Delta t = 1$ ms (as a reference), respectively.

Table 2 shows the time dispersion upper limits for different schemes when $|\theta(\omega, \Delta t) - \omega\Delta t| < 5 \times 10^{-4}$. Obviously, Iwatsu-A has the largest dispersion upper limit among the five schemes, as shown in Table 2. Meanwhile, we can see that MLA has a smaller time-dispersion error at high frequency and large temporal interval (when $\omega\Delta t \geq 1.85$) than Iwatsu-A does, as shown in Fig. 1(b) and 1(c). Within the stability conditions, a coarse temporal interval always means less computational cost than a fine one does, especially for long-term simulations. The main drawback of using a coarse temporal interval is that we would encounter a serious problem associated with strong artifacts caused by the time dispersion. Here, we focus on eliminating the time-dispersion error caused by a coarse temporal interval; thus, we select MLA scheme since it has the largest stability upper limit among all four third-order symplectic integration schemes listed (i.e., Ruth, Iwatsu-A, Iwatsu-B, and MLA).

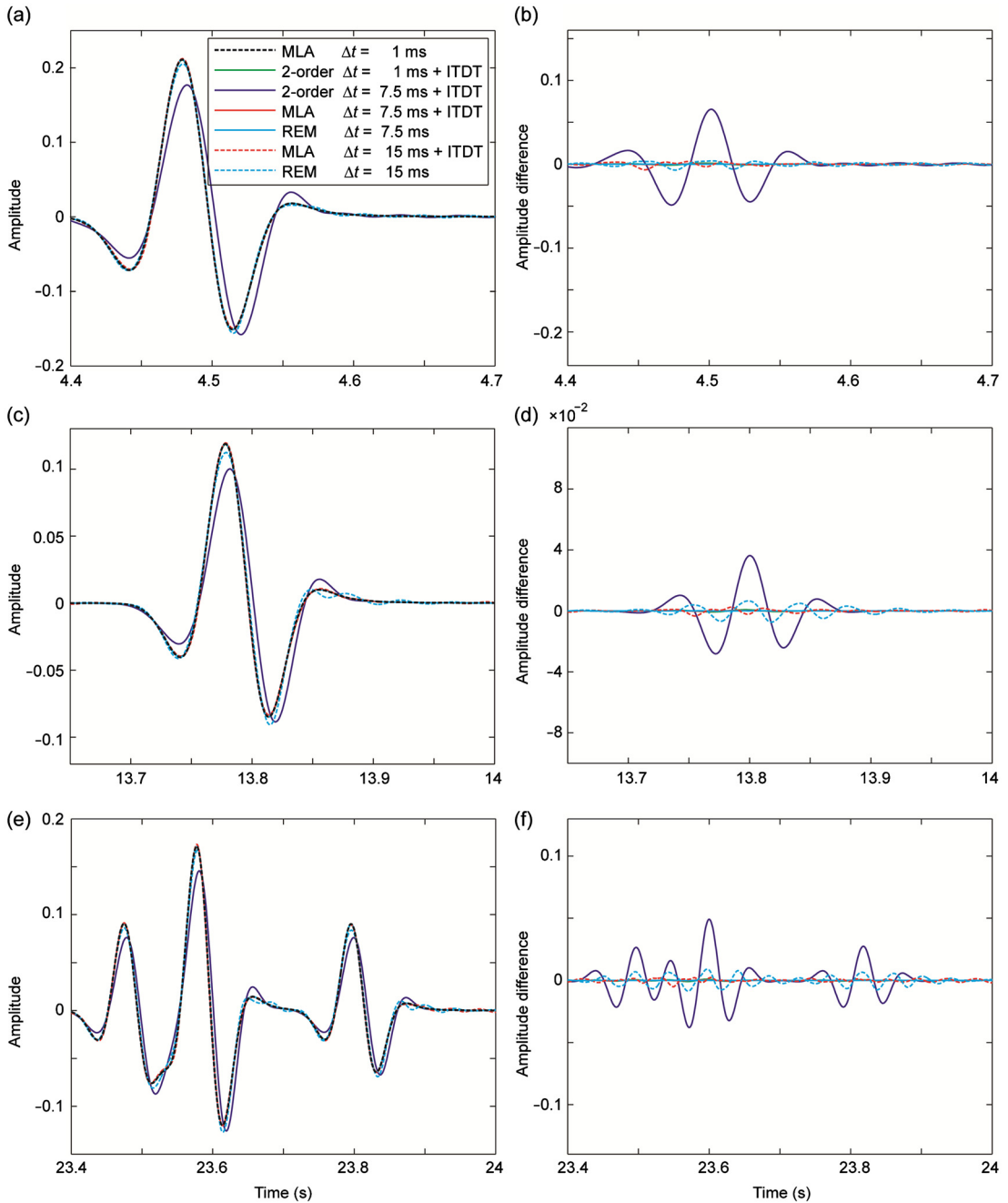


Fig. 3. Waveforms and the amplitude errors after applying the ITDT. This figure is the same as Fig. 2 except that the ITDT has been applied.

Numerical modeling results usually suffer from time-dispersion error, especially for long-term simulations. This time-dispersion error can be predicted by a forward time dispersion transform [51,52]; thus, we can reduce time-dispersion error by employing the ITDT after numerical modeling. As a post-processing method, the ITDT is applied to each numerically calculated time trace $u(t)$ in three steps as follows [51]:

- (a) calculating $\theta(\omega, \Delta t)$ by equation (10) for valid frequencies;
- (b) applying the transform: $\hat{u}'(\omega) = \int u(t) e^{-i[\theta(\omega, \Delta t)/\Delta t]t} dt$;
- (c) applying the inverse Fourier transform: $u'(t) = \frac{1}{2\pi} \int \hat{u}'(\omega) e^{i\omega t} d\omega$,

and the trace $u'(t)$ corrected by the ITDT can be obtained.

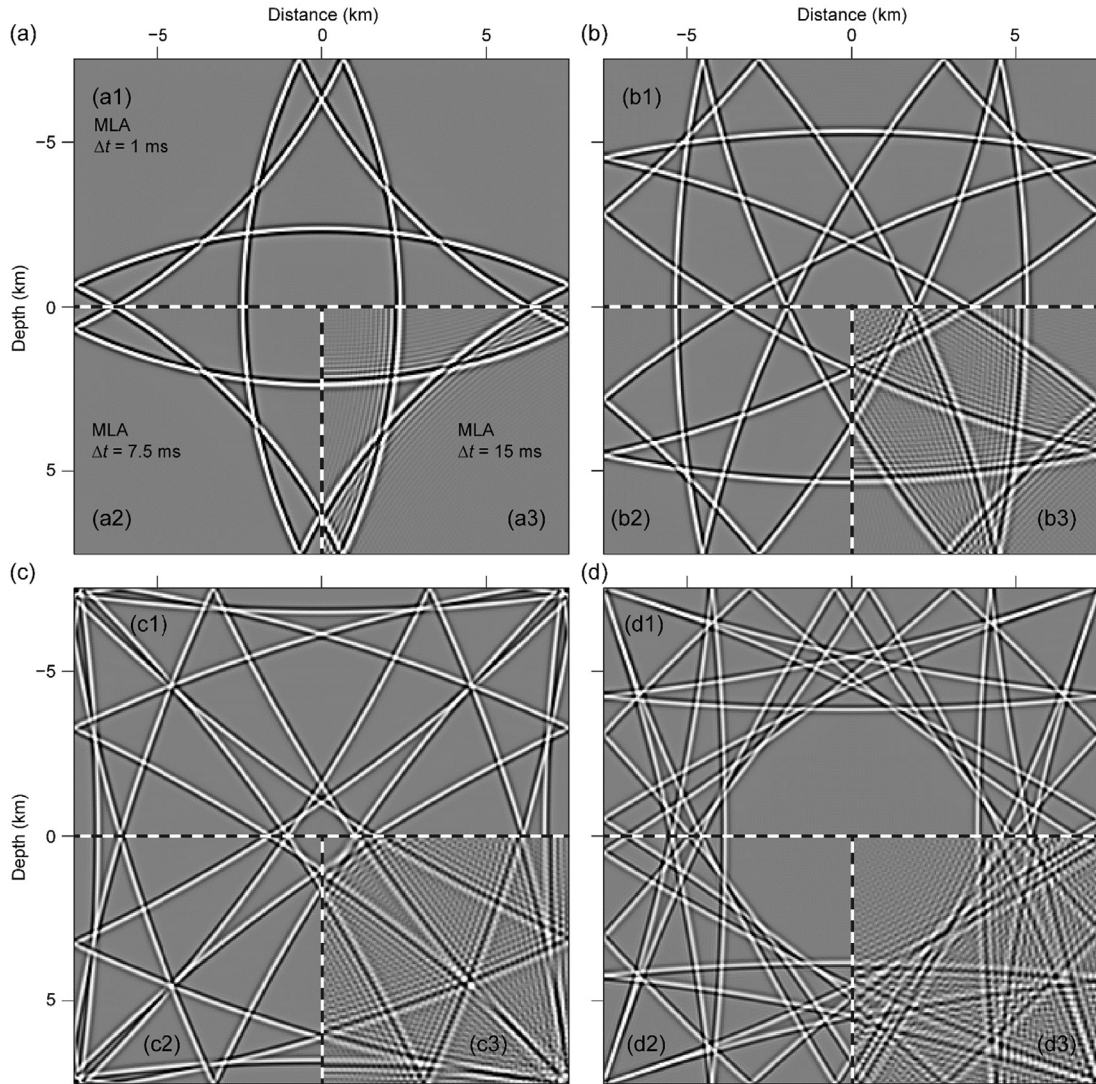


Fig. 4. Snapshots obtained by MLA using different temporal intervals. (a)–(d) are the snapshots at 6, 12, 18, and 24 s, respectively. (a1), (b1), (c1), and (d1) are obtained using $\Delta t = 1$ ms. (a2), (b2), (c2), and (d2) are obtained using $\Delta t = 7.5$ ms. (a3), (b3), (c3), and (d3) are obtained using $\Delta t = 15$ ms.

Step (b) can be regarded as a modified version of the Fourier transform, where ω is replaced by $\theta(\omega, \Delta t)/\Delta t$. As shown in equation (10), $\theta(\omega, \Delta t)$ is the newly defined phase shift, which can truly reflect the influence caused by the temporal discretization; thus, the time-dispersion error $\theta(\omega, \Delta t) - \omega\Delta t$ can be reduced by using this modified transform. A taper function should be used on both ends of the trace to avoid Gibbs phenomena. Usually, a Hanning window with 200 points is good enough in empirical (i.e., 100 points for each end).

6. Numerical experiments

We perform numerical experiments on a homogeneous medium. Three schemes are selected: MLA, 2-order, and the rapid expansion method (REM) [40]. The wave velocity of a square model is $v = 3000$ m/s. The spatial grid interval is $\Delta x = \Delta z = 50$ m, and the grid number is 301×301 . The source is a Ricker wavelet with a dominant frequency of 10 Hz, and the source is located at $x = 0$ m and $z = 0$ m. Using the velocity $v = 3000$ m/s and spatial grid interval $\Delta x = 50$ m, we can obtain the maximum temporal intervals for MLA and 2-order based on the stability upper limits shown in Table 2. The maximum temporal intervals for MLA and 2-order are 16.97 and 7.50 ms, respectively. We test several different temporal intervals: $\Delta t = 1$ and 7.5 ms for 2-order, $\Delta t = 7.5$ and 15 ms for both MLA and REM. The total length of travel time for each method is 26 s.

The time-dispersion error decreases as the temporal interval becomes smaller. This indicates that a smaller temporal interval can obtain more accurate simulation results [56]. To examine the results obtained by different methods, we per-

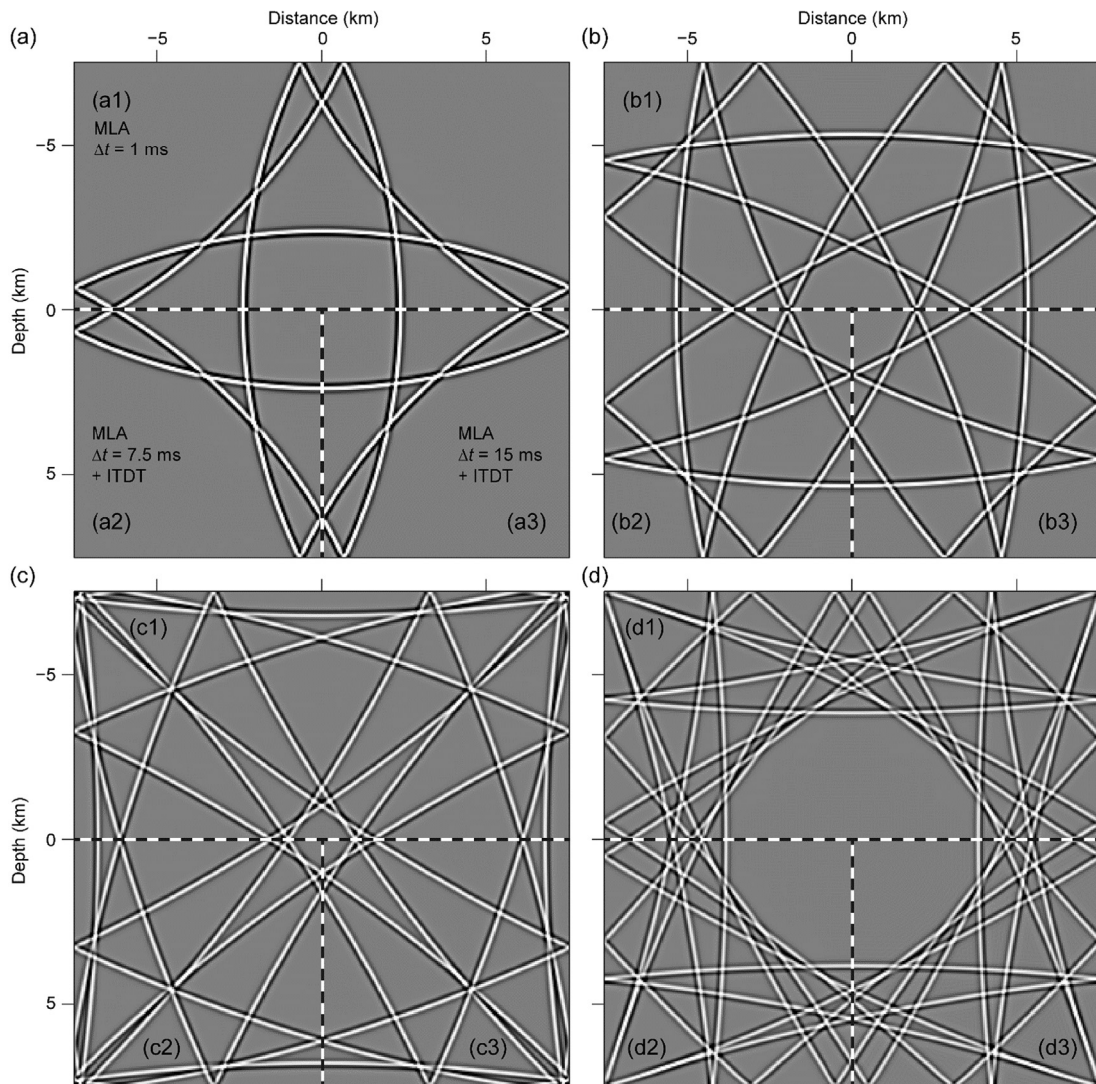


Fig. 5. Snapshots obtained by MLA using different temporal intervals after applying the ITDT. This figure is the same as Fig. 4 except that the ITDT has been applied.

formed numerical simulations by MLA with a temporal interval $\Delta t = 1$ ms, which can be regarded as a theoretical reference to examine the accuracy using larger temporal intervals.

We recorded a trace at a fixed point ($x = -3000$ m, $z = 3000$ m). Figs. 2(a), 2(c), and 2(e) show the waveforms over the time around 4.5, 13.8, and 23.7 s, respectively; Figs. 2(b), 2(d), and 2(f) show the amplitude errors of different schemes using different Δt (where the reference waveform is obtained by MLA with $\Delta t = 1$ ms). For the same scheme, we can see that the time-dispersion error for a large temporal interval (e.g. MLA with $\Delta t = 15$ ms) is more apparent than a small temporal interval (e.g. MLA with $\Delta t = 7.5$ ms); meanwhile, the time-dispersion error becomes more and more serious with an increasing length of travel time. When $\Delta t = 7.5$ ms, 2-order is the poorest and REM is the best among all methods without applying the ITDT. When $\Delta t = 15$ ms, REM has visible time-dispersion error while MLA has apparent time-dispersion error, as shown in Fig. 2(f). 2-order does not work when $\Delta t = 15$ ms since its maximum temporal interval according to the stability upper limit is only 7.50 ms. Even when $\Delta t = 1$ ms, 2-order has fairly large time-dispersion error, which is worse than that of MLA with $\Delta t = 7.5$ ms; in contrast, REM has no visible time-dispersion error with $\Delta t = 7.5$ ms.

Fig. 3 shows the waveforms and the amplitude errors of different methods after applying the ITDT. Obviously, the time-dispersion error has been almost perfectly eliminated and the residual error is fairly weak, except for 2-order with $\Delta t = 7.5$ ms. MLA with $\Delta t = 15$ ms after applying the ITDT is more accurate than REM with $\Delta t = 15$ ms. The result of 2-order with $\Delta t = 7.5$ ms corrected by the ITDT show that 2-order, even applying the ITDT, is not suitable for long-term simulations with a coarse temporal interval. In contrast, the third-order symplectic integration methods applying the ITDT are more suitable for long-term simulations because of their low time-dispersion error.

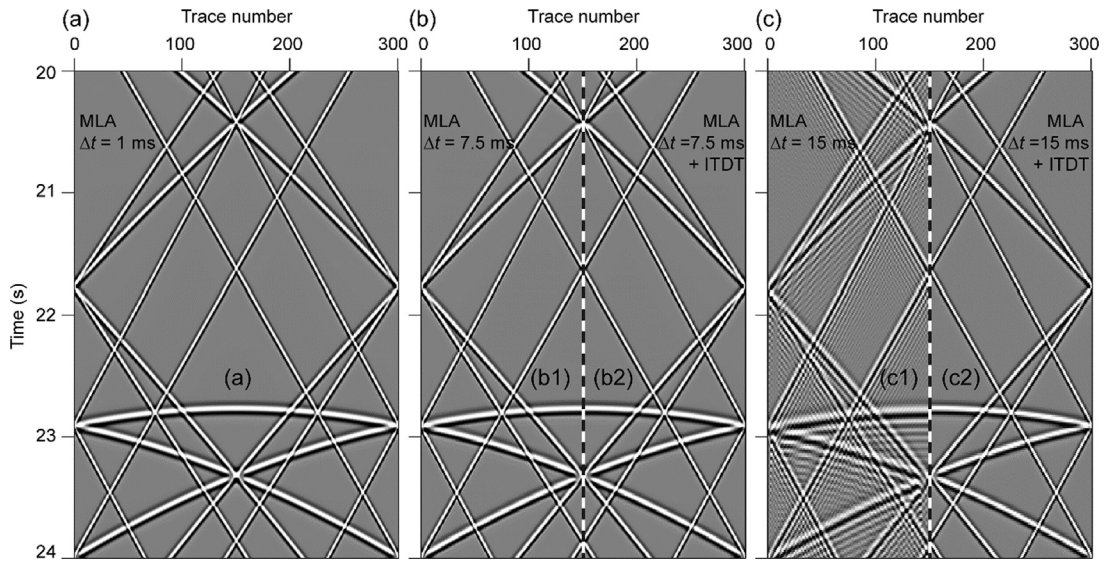


Fig. 6. Comparison between the records before and after applying the ITDT. The records are obtained on the ground surface using MLA with different temporal intervals.

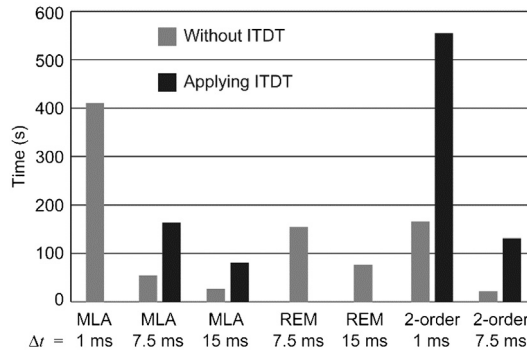


Fig. 7. Comparison between the running times using different schemes with different temporal intervals before and after applying the ITDT.

Fig. 4 shows the snapshots obtained by MLA using different temporal intervals. Figs. 4(a) to 4(d) are the snapshots at 6, 12, 18, and 24 s, respectively. No visible time dispersion appears in the results obtained by temporal interval $\Delta t = 1$ and 7.5 ms. In contrast, the time-dispersion error becomes apparent in the wavefield computed by $\Delta t = 15$ ms, as shown in Figs. 4(a3), 4(b3), 4(c3), and 4(d3). Fig. 5 shows the snapshots obtained by MLA using different temporal intervals after applying the ITDT. Obviously, the time-dispersion error of MLA with $\Delta t = 15$ ms is invisible after applying the ITDT.

The records obtained on the ground surface further illustrate the performance of the ITDT on reducing the time-dispersion error for various schemes with different temporal intervals, as shown in Fig. 6. Obviously, we can see that MLA with $\Delta t = 15$ ms involve heavy time dispersion especially at long travel times, since they are far away from the reference waveforms. In contrast, after we apply the ITDT to these numerical simulation results, the time-dispersion error can be significantly reduced. These numerical experiments show that the ITDT is a powerful tool for improving the numerical accuracy of the third-order symplectic integration method.

Up to now, the ITDT has shown to be effective on reducing time dispersion. In terms of numerical implementation, however, half of the ITDT could not be implemented effectively since there is no fast algorithm available. Fortunately, the other half of the ITDT would be very fast since it can take advantage of the fast Fourier transform. In fact, it is not necessary to perform the ITDT on all traces. We can only perform the ITDT on those traces for output. This is convenient for numerical simulation since we seldom care about the whole volume of wavefields propagating in the entire model set. On the other hand, a larger temporal interval can be used after we apply the ITDT, which would save a large number of iteration times; thus, the total computational efficiency would be much higher for long-term problems. Fig. 7 shows the comparison between the running times using different schemes with different temporal intervals before and after applying the ITDT. The results obtained by MLA with $\Delta t = 15$ ms after applying the ITDT are better than those obtained by 2-order with $\Delta t = 7.5$ ms after applying the ITDT, as shown in Figs. 3(b), 3(d), and 3(f); whereas, the running time of the former is smaller than that

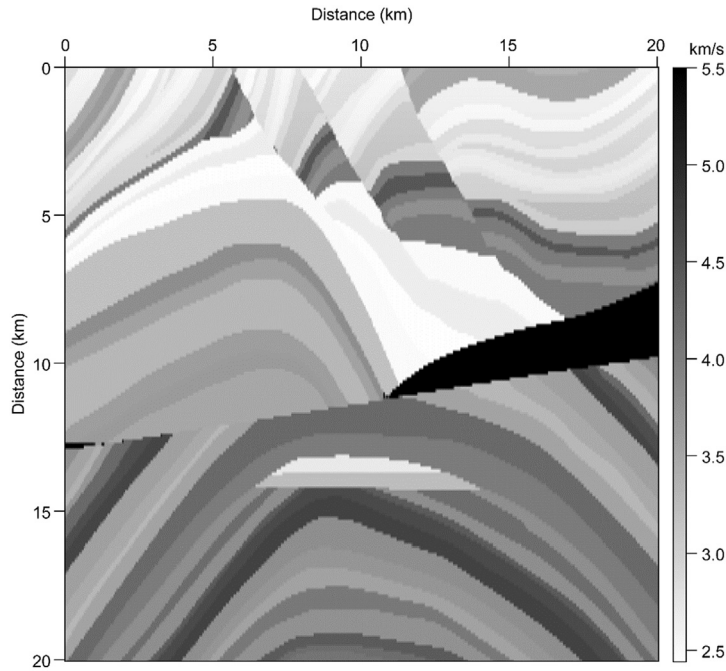


Fig. 8. Modified Marmousi model.

of the latter. In addition, with almost the same running time, the results obtained by MLA with $\Delta t = 15$ ms after applying the ITDT are better than those obtained by REM with $\Delta t = 15$ ms.

We test the numerical simulation results for a heterogeneous medium, Marmousi model, which is popular in examining the accuracy of numerical methods for wave propagating in complex structures. In Marmousi model, the velocity contrast is strong and the multiples are significant. The velocity range of the complete Marmousi model is from 1500 to 5500 m/s. A Ricker wavelet with a dominant frequency of 10 Hz is used as source, and the source is located at the center of the model. With the grid size $\Delta x = \Delta z = 50$ m, numerical experiments show that apparent artifacts arise in low velocity regions, which would influence the time dispersion. Therefore, we clip the Marmousi model (as shown in Fig. 8) by leaving the minimum velocity of 2440 m/s. The grid number of the model is 401×401 . The maximum temporal intervals for MLA and 2-order are 9.25 and 4.09 ms, respectively. We use $\Delta t = 9$ and 4 ms instead for the convenience of numerical comparison. The waveform is recorded at $x = 1750$ m and $z = 1750$ m, and the total length of travel time is ~ 210 seconds.

As shown in Fig. 9, the time dispersion is serious at 200 seconds for 2-order with $\Delta t = 1$ and 4 ms. The ITDT can almost perfectly eliminate time-dispersion error when $\Delta t = 1$ ms; meanwhile, it can significantly reduce time-dispersion error when $\Delta t = 4$ ms. The results obtained by REM are accurate when $\Delta t = 1$ ms but have obvious travel time error when $\Delta t = 4$ ms. The time dispersion is strong for MLA with $\Delta t = 9$ ms, but it is almost perfectly corrected after applying the ITDT. Obviously, our method is feasible for such an ultra-long travel time, which is ~ 40 times as big as general cases (~ 5 seconds for most practical applications). This shows that our scheme is helpful for overcoming the time dispersion caused by coarse temporal interval at ultra-long travel time, for both primary and multiple arrivals.

7. Conclusions

The symplectic integration method is a traditional high-accuracy numerical scheme for modeling of the acoustic wave equation. However, it still suffers from the time-dispersion error for long-term simulation. We incorporate the inverse time dispersion transform (ITDT) into the third-order symplectic integration method to reduce its time-dispersion error. Both theoretical analyses and numerical experiments show that the ITDT is powerful and significant in eliminating time-dispersion error caused by the symplectic integration method, especially at long travel times. The ITDT allows us to use a much larger temporal interval which is close to the upper limit under stability conditions. This means that we can save a large number of iteration times by using the coarsest temporal interval without suffering from the time dispersion. Therefore, the total computational efficiency after using the ITDT only has a slight increase compared with the original method using small temporal interval and could be even faster.

Acknowledgements

This research was supported by the National Natural Science Foundation of China (Grant No. 41130418) and the National Major Project of China (Grant No. 2011ZX05008-006).

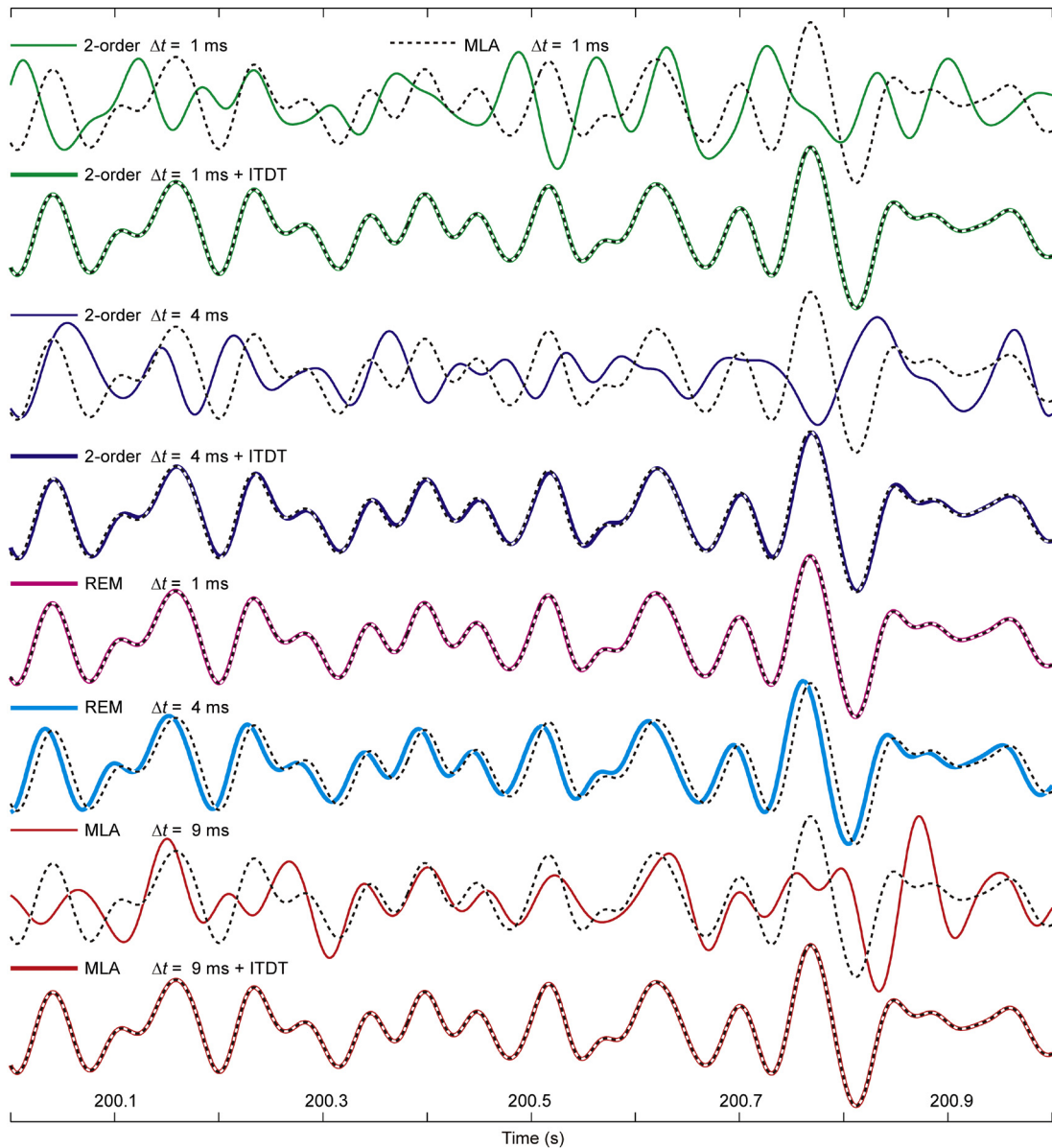


Fig. 9. Waveform comparison between different methods. An ultra-long travel time ~ 210 seconds is applied. The black dashed lines denote the reference waveforms obtained by MLA using $\Delta t = 1$ ms, which can be regarded as analytical solutions.

References

- [1] J.M. Carcione, G.C. Herman, A. Ten Kroode, Seismic modeling, *Geophysics* 67 (2002) 1304–1325.
- [2] Z. Alterman, F. Karal, Propagation of elastic waves in layered media by finite difference methods, *Bull. Seismol. Soc. Am.* 58 (1968) 367–398.
- [3] R. Alford, K. Kelly, D.M. Boore, Accuracy of finite-difference modeling of the acoustic wave equation, *Geophysics* 39 (1974) 834–842.
- [4] J. Virieux, SH-wave propagation in heterogeneous media: velocity-stress finite-difference method, *Geophysics* 49 (1984) 1933–1942.
- [5] J. Gazdag, Modeling of the acoustic wave equation with transform methods, *Geophysics* 46 (1981) 854–859.
- [6] D.D. Kosloff, E. Baysal, Forward modeling by a Fourier method, *Geophysics* 47 (1982) 1402–1412.
- [7] D.D. Kosloff, M. Reshef, D. Loewenthal, Elastic wave calculations by the Fourier method, *Bull. Seismol. Soc. Am.* 74 (1984) 875–891.
- [8] B. Fornberg, The pseudospectral method: comparisons with finite differences for the elastic wave equation, *Geophysics* 52 (1987) 483–501.
- [9] K.J. Marfurt, Accuracy of finite-difference and finite-element modeling of the scalar and elastic wave equations, *Geophysics* 49 (1984) 533–549.
- [10] D. Komatitsch, J.-P. Vilotte, The spectral element method: an efficient tool to simulate the seismic response of 2D and 3D geological structures, *Bull. Seismol. Soc. Am.* 88 (1998) 368–392.
- [11] E. Dormy, A. Tarantola, Numerical simulation of elastic wave propagation using a finite volume method, *J. Geophys. Res., Solid Earth* (1978–2012) 100 (1995) 2123–2133.
- [12] M.A. Dablain, The application of high-order differencing to the scalar wave equation, *Geophysics* 51 (1986) 54–66.
- [13] J.T. Etgen, High-order finite-difference reverse time migration with the 2-way non-reflecting wave equation, Stanford Exploration Project, Report-48 1986, pp. 133–146.

- [14] J.T. Etgen, Evaluating finite-difference operators applied to wave simulation, Stanford Exploration Project, Report-57, 1988, pp. 243–258.
- [15] Y. Liu, M.K. Sen, A new time-space domain high-order finite-difference method for the acoustic wave equation, *J. Comput. Phys.* 228 (2009) 8779–8806.
- [16] Y. Liu, M.K. Sen, Time-space domain dispersion-relation-based finite-difference method with arbitrary even-order accuracy for the 2D acoustic wave equation, *J. Comput. Phys.* 232 (2013) 327–345.
- [17] O. Holberg, Computational aspects of the choice of operator and sampling interval for numerical differentiation in large-scale simulation of wave phenomena, *Geophys. Prospect.* 35 (1987) 629–655.
- [18] J.T. Etgen, A tutorial on optimizing time domain finite-difference schemes: “Beyond Holberg”, Stanford Exploration Project, Report-129, 2007, pp. 33–43.
- [19] H. Zhou, G. Zhang, Prefactored optimized compact finite-difference schemes for second spatial derivatives, *Geophysics* 76 (2011) WB87–WB95.
- [20] C. Chu, P.L. Stoffa, Determination of finite-difference weights using scaled binomial windows, *Geophysics* 77 (2012) W17–W26.
- [21] J. Zhang, Z. Yao, Optimized explicit finite-difference schemes for spatial derivatives using maximum norm, *J. Comput. Phys.* 250 (2013) 511–526.
- [22] J. Zhang, Z. Yao, Optimized finite-difference operator for broadband seismic wave modeling, *Geophysics* 78 (2013) A13–A18.
- [23] Y. Liu, Globally optimal finite-difference schemes based on least squares, *Geophysics* 78 (2013) T113–T132.
- [24] S. Tan, L. Huang, A staggered-grid finite-difference scheme optimized in the time-space domain for modeling scalar-wave propagation in geophysical problems, *J. Comput. Phys.* 276 (2014) 613–634.
- [25] Y. Wang, W. Liang, Z. Nashed, X. Li, G. Liang, C. Yang, Seismic modeling by optimizing regularized staggered-grid finite-difference operators using a time-space-domain dispersion-relationship-preserving method, *Geophysics* 79 (2014) T277–T285.
- [26] W. Sun, B. Zhou, L.Y. Fu, A staggered-grid convolutional differentiator for elastic wave modelling, *J. Comput. Phys.* 301 (2015) 59–76.
- [27] J.P. Boris, D.L. Book, Flux-corrected transport. I. SHASTA, a fluid transport algorithm that works, *J. Comput. Phys.* 11 (1973) 38–69.
- [28] T. Fei, K. Larner, Elimination of numerical dispersion in finite-difference modeling and migration by flux-corrected transport, *Geophysics* 60 (1995) 1830–1842.
- [29] D. Yang, E. Liu, Z. Zhang, J. Teng, Finite-difference modelling in two-dimensional anisotropic media using a flux-corrected transport technique, *Geophys. J. Int.* 148 (2002) 320–328.
- [30] D. Yang, J. Teng, Z. Zhang, E. Liu, A nearly analytic discrete method for acoustic and elastic wave equations in anisotropic media, *Bull. Seismol. Soc. Am.* 93 (2003) 882–890.
- [31] D. Yang, M. Lu, R. Wu, J. Peng, An optimal nearly analytic discrete method for 2D acoustic and elastic wave equations, *Bull. Seismol. Soc. Am.* 94 (2004) 1982–1991.
- [32] P. Tong, D. Yang, B. Hua, M. Wang, A high-order stereo-modeling method for solving wave equations, *Bull. Seismol. Soc. Am.* 103 (2013) 811–833.
- [33] P.L. Stoffa, R.C. Pestana, Numerical solution of the acoustic wave equation by the rapid expansion method (REM) – a one step time evolution algorithm, in: 79th Annual International Meeting, SEG, Expanded Abstracts, Society of Exploration Geophysicists, 2009, pp. 2672–2676.
- [34] J.B. Chen, High-order time discretizations in seismic modeling, *Geophysics* 72 (2007) SM115–SM122.
- [35] Y. Zhang, G. Zhang, D. Yingst, J. Sun, Explicit marching method for reverse time migration, in: 77th Annual International Meeting, SEG, Expanded Abstracts, Society of Exploration Geophysicists, 2007, pp. 2300–2304.
- [36] R. Soubaras, Y. Zhang, Two-step explicit marching method for reverse time migration, in: 78th Annual International Meeting, SEG, Expanded Abstracts, Society of Exploration Geophysicists, 2008.
- [37] Y. Zhang, G. Zhang, One-step extrapolation method for reverse time migration, *Geophysics* 74 (2009) A29–A33.
- [38] H. Tal-Ezer, D. Kosloff, Z. Koren, An accurate scheme for seismic forward modelling, *Geophys. Prospect.* 35 (1987) 479–490.
- [39] D. Kosloff, A. Queiroz Filho, E. Tessmer, A. Behle, Numerical solution of the acoustic and elastic wave equations by a new rapid expansion method, *Geophys. Prospect.* 37 (1989) 383–394.
- [40] R.C. Pestana, P.L. Stoffa, Time evolution of the wave equation using rapid expansion method, *Geophysics* 75 (2010) T121–T131.
- [41] E. Tessmer, Using the rapid expansion method for accurate time-stepping in modeling and reverse-time migration, *Geophysics* 76 (2011) S177–S185.
- [42] S. Fomel, L. Ying, X. Song, Seismic wave extrapolation using lowrank symbol approximation, in: 80th Annual International Meeting, SEG, Expanded Abstracts, Society of Exploration Geophysicists, 2010.
- [43] S. Fomel, L. Ying, X. Song, Seismic wave extrapolation using lowrank symbol approximation, *Geophys. Prospect.* 61 (2012) 526–536.
- [44] X. Song, S. Fomel, Fourier finite-difference wave propagation, *Geophysics* 76 (2011) T123–T129.
- [45] X. Song, K. Nihei, J. Stefani, Seismic modeling in acoustic variable-density media by Fourier finite differences, in: 82th Annual International Meeting, SEG, Expanded Abstracts, Society of Exploration Geophysicists, 2012.
- [46] X. Song, S. Fomel, L. Ying, Lowrank finite-differences and lowrank Fourier finite-differences for seismic wave extrapolation in the acoustic approximation, *Geophys. J. Int.* 193 (2013) 960–969.
- [47] Y.E. Li, M. Wong, R. Clapp, Equivalent accuracy at a fraction of the cost: overcoming temporal dispersion, Stanford Exploration Project, Report-150, 2013.
- [48] C. Stork, Eliminating nearly all dispersion error from FD modeling and RTM with minimal cost increase, in: 75th Annual International Conference and Exhibition, EAGE, Extended Abstracts, Tu 11 07, 2013.
- [49] H. Liu, N. Dai, F. Niu, W. Wu, An explicit time evolution method for acoustic wave propagation, *Geophysics* 79 (2014) T117–T124.
- [50] N. Dai, H. Liu, W. Wu, Solutions to numerical dispersion error of time FD in RTM, in: 84th Annual International Meeting, SEG, Expanded Abstracts, Society of Exploration Geophysicists, 2014, pp. 4027–4031.
- [51] M. Wang, S. Xu, Finite-difference time dispersion transforms for wave propagation, *Geophysics* 80 (2015) WD19–WD25.
- [52] M. Wang, S. Xu, Time dispersion prediction and correction for wave propagation, in: 85th Annual International Meeting, SEG, Expanded Abstracts, Society of Exploration Geophysicists, 2015, pp. 3677–3681.
- [53] J.B. Chen, Lax-Wendroff and Nyström methods for seismic modelling, *Geophys. Prospect.* 57 (2009) 931–941.
- [54] E.J. Nyström, Über die numerische Integration von Differentialgleichungen (Mitgeteilt am 23 Sept. 1925 von E. Lindelöf und K.F. Sundman), *Societas scientiarum Fennica*, 1925.
- [55] E. Hairer, S.P. Nørsett, G. Wanner, *Solving Ordinary Differential Equations I: Nonstiff Problems*, Springer, Berlin, 1993.
- [56] J.B. Chen, Modeling the scalar wave equation with Nyström methods, *Geophysics* 71 (2006) T151–T158.
- [57] R.D. Ruth, A canonical integration technique, *IEEE Trans. Nucl. Sci.* 30 (1983) 2669–2671.
- [58] H. Yoshida, Construction of higher order symplectic integrators, *Phys. Lett. A* 150 (1990) 262–268.
- [59] M.Z. Qin, M.Q. Zhang, Multi-stage symplectic schemes of two kinds of Hamiltonian systems for wave equations, *Comput. Math. Appl.* 19 (1990) 51–62.
- [60] J.B. Chen, H. Liu, Optimization approximation with separable variables for the one-way wave operator, *Geophys. Res. Lett.* 31 (2004) L06613.
- [61] G. Fang, S. Fomel, Q. Du, J. Hu, Lowrank seismic-wave extrapolation on a staggered grid, *Geophysics* 79 (2014) T157–T168.
- [62] J.T. Etgen, S. Brandsberg-Dahl, The pseudo-analytical method: application of pseudo-Laplacians to acoustic and acoustic anisotropic wave propagation, in: 79th Annual International Meeting, SEG, Expanded Abstracts, Society of Exploration Geophysicists, 2009, pp. 2552–2556.
- [63] X. Li, W. Wang, M. Lu, M. Zhang, Y. Li, Structure-preserving modelling of elastic waves: a symplectic discrete singular convolution differentiator method, *Geophys. J. Int.* 188 (2012) 1382–1392.
- [64] D. Komatitsch, J. Tromp, Spectral-element simulations of global seismic wave propagation – II. Three-dimensional models, oceans, rotation and self-gravitation, *Geophys. J. Int.* 150 (2002) 303–318.

- [65] S. Liu, X. Li, W. Wang, Y. Liu, M. Zhang, H. Zhang, A new kind of optimal second-order symplectic scheme for seismic wave simulations, *Sci. China Earth Sci.* 44 (2014) 283–291 (in Chinese).
- [66] K. Feng, M.Z. Qin, *Symplectic Geometric Algorithms for Hamiltonian Systems*, Zhejiang Science & Technology Press, Hangzhou, China, 2003 (in Chinese).
- [67] X. Ma, D. Yang, F. Liu, A nearly analytic symplectically partitioned Runge–Kutta method for 2-D seismic wave equations, *Geophys. J. Int.* 187 (2011) 480–496.
- [68] R.I. McLachlan, P. Atela, The accuracy of symplectic integrators, *Nonlinearity* 5 (1992) 541–562.
- [69] W. Wang, X. Li, A new solution to the third-order non-gradient symplectic integration algorithm, *Wuhan Univ. J. Nat. Sci.* 58 (2012) 221–228 (in Chinese).
- [70] R. Iwatsu, Two new solutions to the third-order symplectic integration method, *Phys. Lett. A* 373 (2009) 3056–3060.